Terra Nova

Pre-Cenomanian versus Cenozoic folding in the High Atlas revealed by paleomagnetic data

Journal:	*Terra Nova*
Manuscript ID	TER-2015-0032.R2
Wiley - Manuscript type:	Paper
Date Submitted by the Author:	n/a
Complete List of Authors:	Torres López, Sara; Universidad de Burgos, Física Casas, Antonio; Universidad de Zaragoza, Ciencias de la Tierra Villalaín, Juan José; University of Burgos, physics El Ouardi, Hamidou; Université Moulay Ismail, Géologie Moussaid, Bennacer; Université Hassan II, Sciences Naturelles
Keywords:	PALEOMAGNETISM, REMAGNETIZATION, INTRUSION, CENTRAL HIGH ATLAS

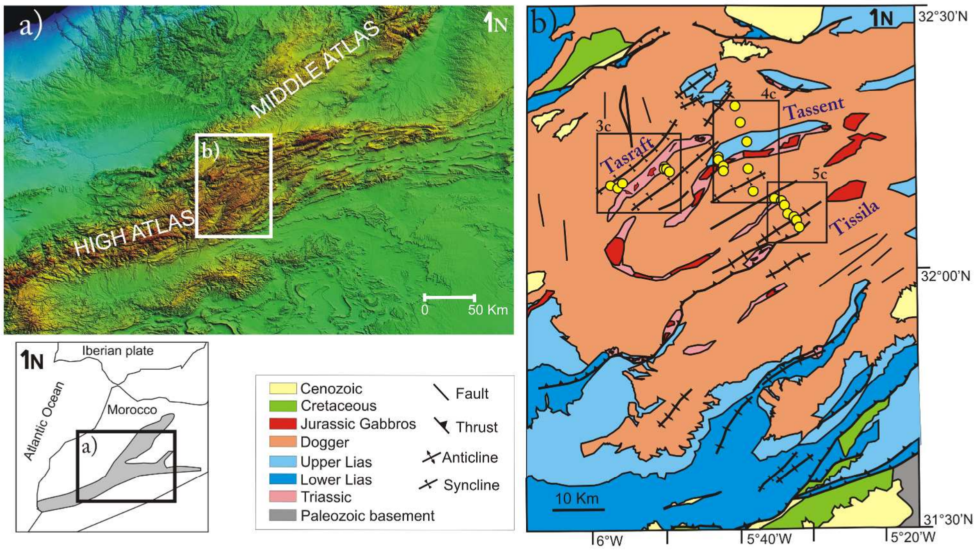

Figure 1. A) DEM and geological sketch with the situation of the Central High Atlas and Imilchil area. B) Geological map of the Imilchil region, the sampling sites and the situation of the three restored profiles corresponding to figures 3, 4 and 5. Modified from Torres-López et al., (2014).

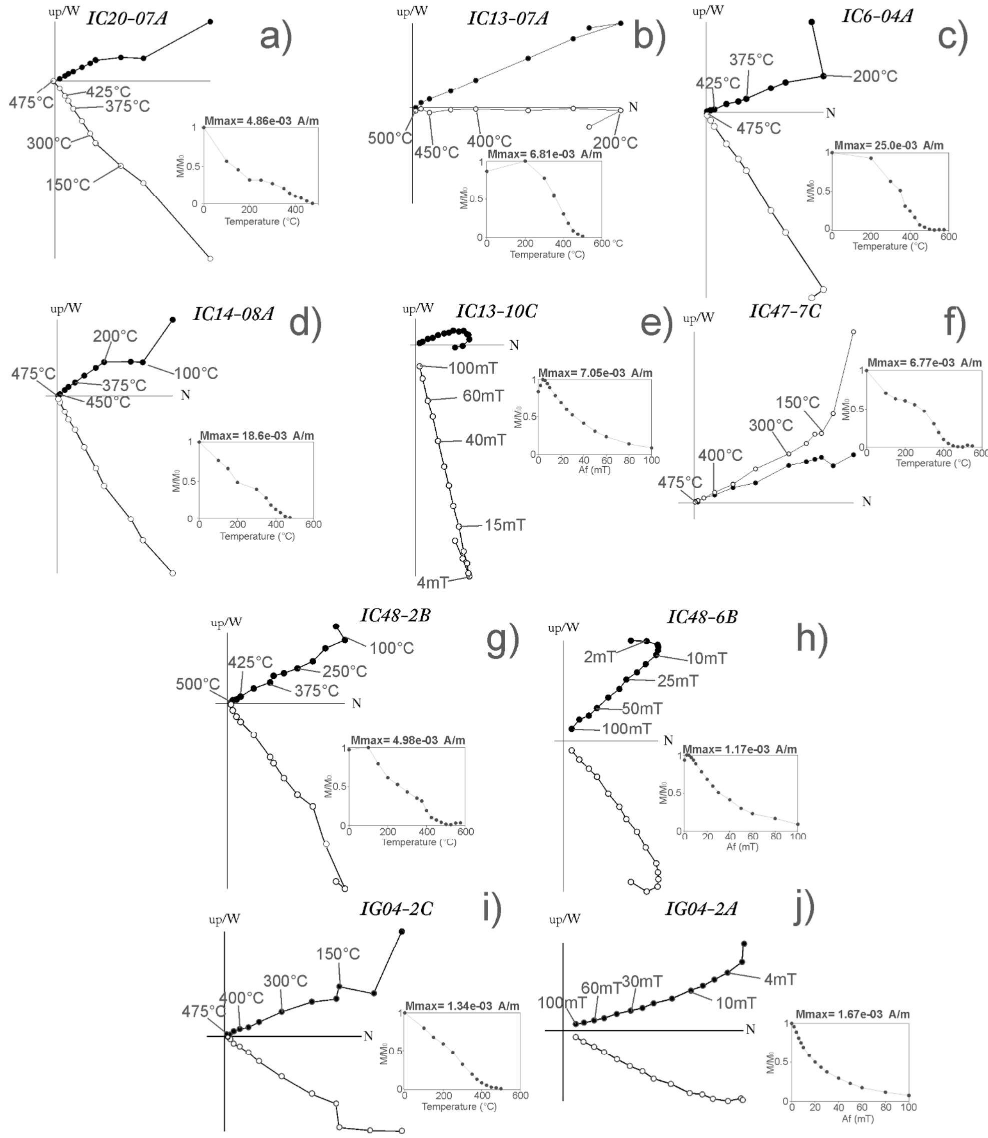

Figure 2. NRM thermal and alternating field demagnetizations of representative samples. All directions are plotted with their in-situ coordinates. Open symbols are projections of the vector end points onto the vertical north–south plane, and filled symbols are projections onto the horizontal plane. The evolution of normalized NRM intensity M/M0 is shown in the insets.

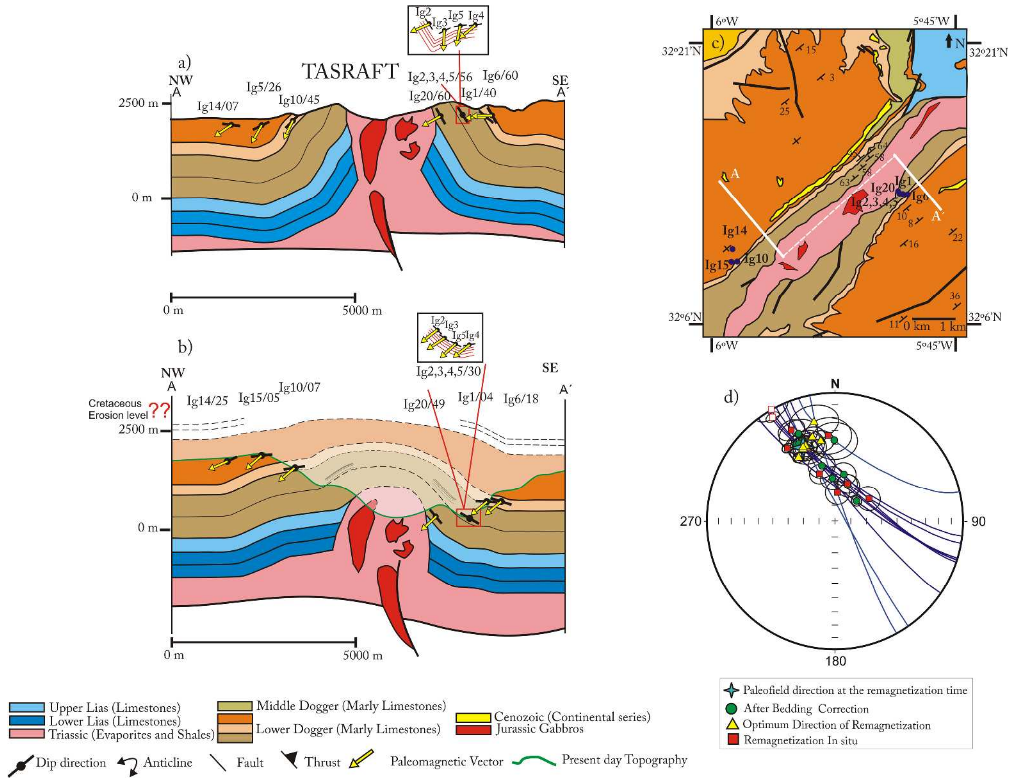

Figure 3. A) Present-day geological profile of the Tasraft anticline. The paleomagnetic sites, bedding (black lines) and paleomagnetic vectors (arrows) are indicated. B) Restored section of the Tasraft anticline to 100 Ma. C) Geological sketch showing the location of the studied transect and the paleomagnetic sites (based on Fadile, 1987). D) Stereoplot showing the small circles corresponding to the restored remagnetization directions from selected sites. Squares are directions of the in situ remagnetization for each site. Triangles represent the optimum directions of remagnetization for each site. Circles show the paleomagnetic direction of remagnetization after complete bedding correction. The 95% confidence circles are also represented. Paleomagnetic vectors have been projected onto the vertical plane of the cross-section, and the inclinations shown in this figure are therefore apparent inclinations. The green line in the restored section represents the restored topography.

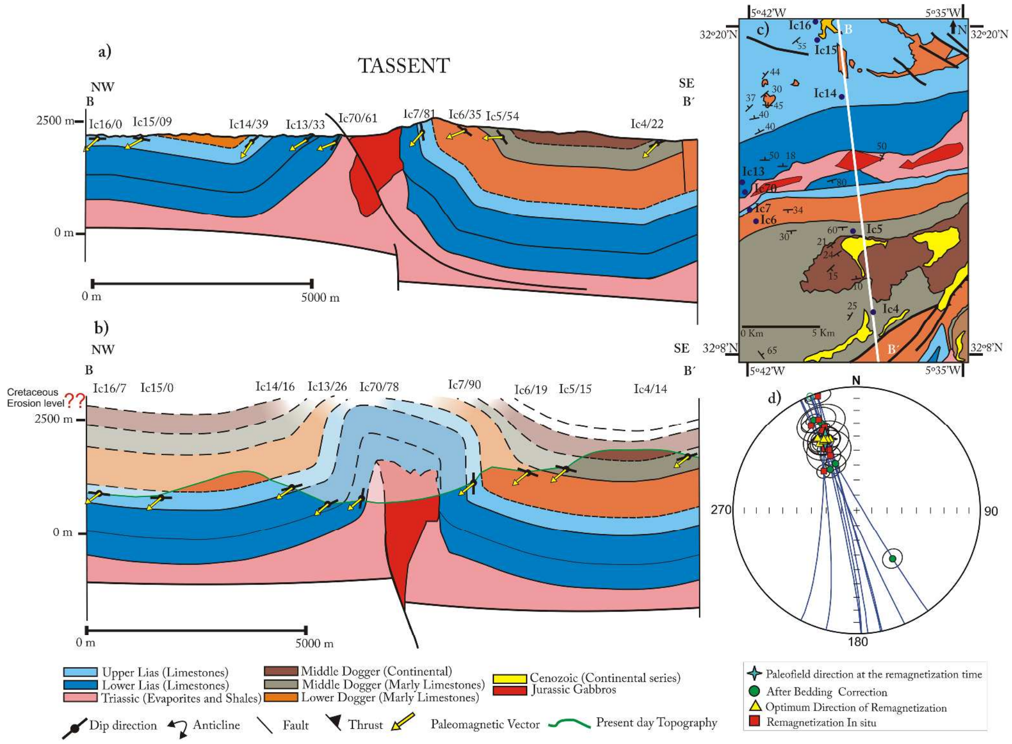

Figure 4. A) Present-day Tassent geological profile. B) Restored section to 100 Ma. C) Geological sketch showing the transect studied and the paleomagnetic sites (based on Fadile 1987). D) Stereoplot showing small circles corresponding to the restored remagnetization directions from selected sites. Symbols are the same as those shown in fig. 3.

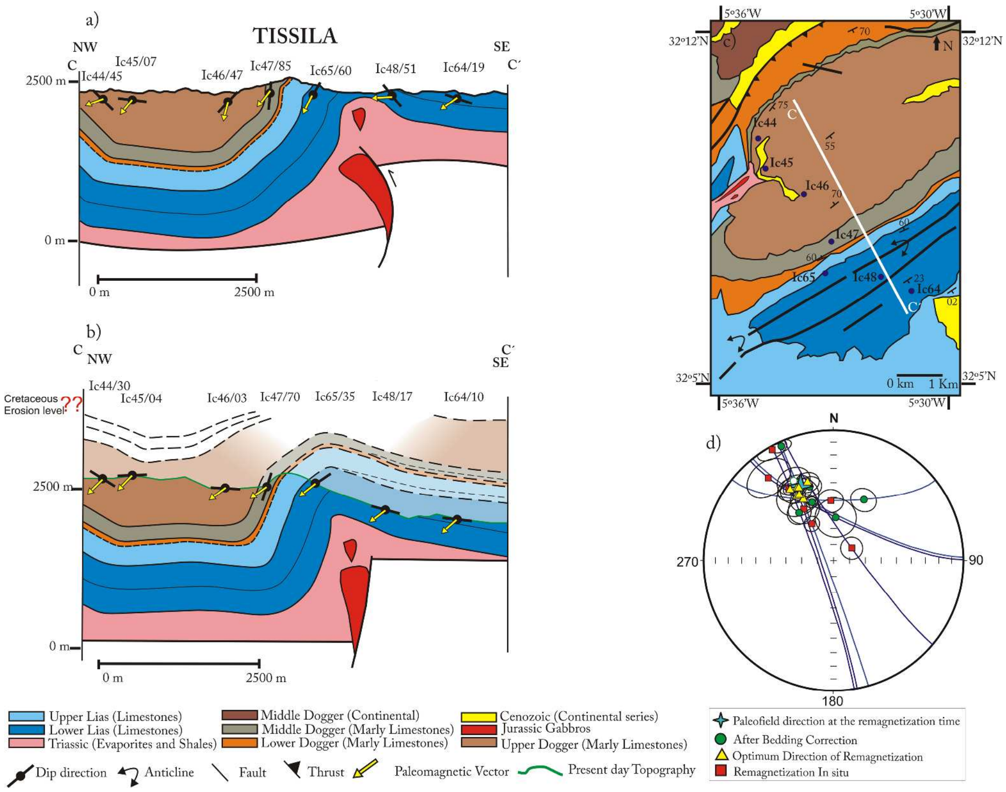

Figure 5. A) Present-day cross-section of the Tissila anticline. The paleomagnetic sites, bedding and paleomagnetic vectors are indicated. B) Restored section to 100 Ma. C) Geological sketch showing the transect studied and the paleomagnetic sites (based on map of Imilchil, Fadile 1987). D) Stereoplot showing the small circles corresponding to the restored remagnetization directions from selected sites. Symbols are the same as those shown in fig. 3.

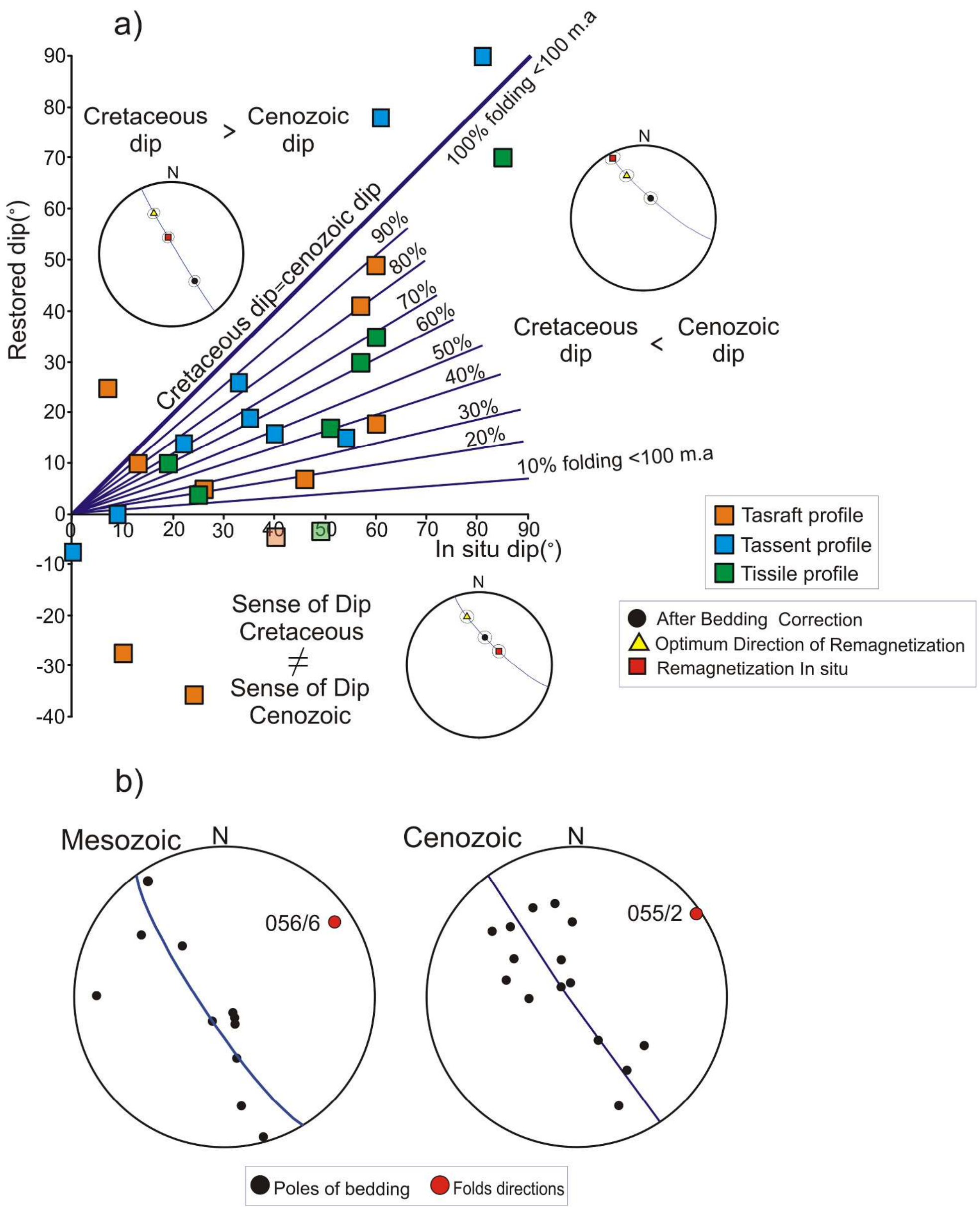

Figure. 6. a) Plot showing the relationship between present-day dips and Cretaceous (~100 Ma) dips at the limbs of the three structures studied in the High Atlas. Points plotted along the abscise axis correspond to those sites whose tilt was totally acquired after the Late Cretaceous (i.e., beds were horizontal before the Cenozoic), and points plotted on the diagonal correspond to sites whose present tilt was acquired before the remagnetization (Late Cretaceous) stage. The distance to the abscise axis is related to the part of the structure that was already formed at the Late Cretaceous. Negative values for the ordinate axis indicate dips during the Late Cretaceous with the dip sense opposite to the present-day, in situ sense of dip. Small equal area diagram showing the optimum direction of the remagnetization, after bedding correction and in situ are also shown for the three cases differentiated in the figure. b) Stereoplots showing the poles to bedding in the Imilchil area (Torres-López et al., 2014) for dips acquired mostly during the pre-inversion stage (i.e. the unfolding for restoration to the paleofield direction is <30% of the present day bedding, left) and for compressional, Cenozoic tilting (i.e. unfolding is >70% of the present day bedding, right). Folds axes obtained are also shown.

Pre-Cenomanian versus Cenozoic folding in the High Atlas revealed by paleomagnetic data

S. Torres-López1*, A. M. Casas2, J. J. Villalaín1, H. EL Ouardi3, B. Moussaid4

1Departamento de Física, Escuela Politécnica Superior, Universidad de Burgos, Avd Cantabria S/N, 09006 Burgos, Spain

2Departamento de Ciencias de la Tierra, Facultad de Ciencias, Universidad de Zaragoza, 50009 Zaragoza, Spain

3Département de Géologie, Faculté des Sciences, Université Moulay Ismail, BP 11201 Zitoune, Meknès, Morocco

4Département des Sciences Naturelles, Ecole Normale supérieure, Université Hassan II, BP : 500 69, Ghandi Casablanca, Morocco

*Corresponding author (e-mail: storres@ubu.es)

Abstract

Paleomagnetic data, and specifically, remagnetizations, are used in this work to constrain the geometric reconstruction at 100 Ma of three anticlines cored by gabbroic intrusions and Triassic shales in the Central High Atlas, Morocco. Previous paleomagnetic results have revealed that the Mesozoic sediments of this region acquired a pervasive remagnetization at the end of the Early Cretaceous. The restoration of paleomagnetic vectors to the remagnetization stage (100 Ma allows one to determine the dip of the beds during this period and, thereby, to obtain a reconstruction of structures during that time and the relative contribution of Mesozoic magmatic/diapiric uplift vs. Cenozoic compression to the present-day dip. The results obtained indicate that three major anticlines in the Central High Atlas (Tasraft, Tassent and Tissila) were initiated to different degrees before the Late Cretaceous and were re-activated during the Cenozoic compression to acquire their present-day geometry. A discussion on the origin of these structures is also presented.

Keywords: paleomagnetism, remagnetization, Central High Atlas, Mesozoic, intrusion, salt tectonics

Introduction

The Atlas belt is an intracontinental chain that developed in Phanerozoic times within the African plate. Whereas its Cenozoic compressional features are relatively well documented because of the record of syn-tectonic deposits at the margins of the belt (Frizon de Lamotte *et al.*, 2008 and references therein; Tesón *et al.*, 2010) and the good outcrop conditions, its tectonic evolution during the Triassic-Jurassic rifting and Cretaceous postrift stage is still controversial. Some authors (Beauchamp *et al.*, 1999; Teixell *et al.*, 2003; Arboleya *et al.*,

2004) consider that folding was very limited in its inner area before the Late Cretaceous and that most folds are the result of Cenozoic compression. Conversely, others favor a partial, if not complete, development of structures in the inner part of the chain predating the Cenozoic compression (Laville and Piqué, 1992; Saura *et al.*, 2014). Regarding the origin of pre-Cenozoic structures, several hypotheses, including Mesozoic compression, strike-slip faulting, diapirism and magmatic intrusions, have been proposed to explain intra-Mesozoic unconformities, cleavage and pre-Cenozoic folding in several parts of the Central High Atlas (Laville *et al.*, 1994, Frizon de Lamotte *et al.*, 2000, 2011; Michard *et al.*, 2008). For instance, plutonic magmatic intrusions (Piqué *et al.*, 2000, and references therein) and Diapirism (Michard *et al.*, 2011; Saura *et al.*, 2014 and references therein) have been invoked as relevant processes that contributed to the Mesozoic evolution of the chain.

In this work, we apply paleomagnetic techniques to obtain a better understanding of the relative chronology of structures and fold evolution in the Central High Atlas. Paleomagnetism can be used to determine the geometry of structures during intermediate stages in basin with several deformational stages (Villalaín *et al.*, 2003; Soto *et al.*, 2008, 2011; Villalaín *et al.*, 2015), provided that a remagnetization stage occurred between these tectonic stages. In basinal areas of the Central High Atlas, this condition is met because of the existence of a recently demonstrated Cretaceous widespread remagnetization occurred at about 100 Ma, affecting Jurassic limestones (Torres-López *et al.*, 2014; Moussaid *et al.*, 2015). The restoration of paleomagnetic vectors to the paleomagnetic reference at the time of remagnetization (100 Ma) allows obtaining the tilting of beds, and therefore a reliable picture of structures at this particular moment, and a relative chronology of tectonic events

Geological framework

The Central High Atlas is an intracontinental fold belt that resulted from the Cenozoic inversion of extensional/transtensional sedimentary basins that developed during Mesozoic times (Laville, 1985; Frizon de Lamotte *et al.*, 2000; Teixell *et al.*, 2003; Arboleya *et al.*, 2004). During the compressional stage, a thick-skinned structural style involving the Palaeozoic co-exists in the inner part of the belt with structures décolled at the Upper Triassic lutitic and evaporitic level. Most structures show a NE to ENE trend, conditioned by Late-Variscan to Triassic large-scale structuring of the region (Laville *et al.*, 2004; El Harfi *et al.*, 2006). Thin-skinned structures, mainly thrusts and thrust-related folds, with opposite vergences at both sides of the chain, developed in the marginal areas having a thinner pre-tectonic, sedimentary cover (Frizon de Lamotte *et al.*, 2008 and references therein).

The study area is characterized by tight anticlines, as the Tassent, Tasraft and Tissila anticlines analysed in detail in this work (Figure 1), flanked by gentle synclines. The cores of the anticlinal ridges are partially occupied by igneous rocks (massive bodies in Tassent and Tasraft) corresponding to Middle-Late Jurassic to Early Cretaceous magmatic event (see

Laville and Piqué, 1992; Armando, 1999; Lhachmi *et al*., 2001; Zayane *et al*., 2002; Guezal *et al*., 2011; Michard *et al*., 2011; Bensalah *et al*., 2013). The igneous core of Tassent anticline crops out along an ENE trending ridge and is surrounded by Upper Triassic shales and Jurassic limestones that become nearly vertical in the proximity to the igneous body. The Tasraft anticline also shows a gabbroic and evaporitic core, having an ENE elongated outcrop following a NE-SW trend, with intermediate dips in the Jurassic limestones at its limbs. Between these structures, the Jurassic units define a gentle syncline. The Tissila anticline, located SE of Tassent (Figure 1) shows an asymmetric shape with northwards vergence. It is cored by Triassic evaporites, and farther East it is in continuity with the igneous core of the Amagmag ridge.

Paleomagnetic methods and results

For this study, we used 20 of the 51 sites that were sampled along the Imilchil cross section by Torres-López *et al*. (2014) as well as 6 new sites. The sites are distributed along three cross sections and throughout the small- and large-scale folds cored by gabbro outcrops, and consist of Toarcian-Bathonian limestones.

All paleomagnetic analyses were conducted in the Paleomagnetic Laboratory of the University of Burgos (Spain). The thermal demagnetization for sites was processed in steps up to 550°C; using a TD48-SC thermal demagnetizer. The Natural Remanent Magnetization

(NRM) of 185 samples was measured using a 2G-755 cryogenic magnetometer. Moreover, pilot samples were demagnetized by alternating fields (AF) technique. The distribution of directions was determined using Fisher's (1953) statistics. Linear regression techniques were used to calculate the directions of the observed components.

The 26 analyzed sites show uniform magnetic properties with magnetic susceptibility values between 100 and 400×10^{-6} (S.I.). The intensity of the NRM is between 1 and 80 mA/m. Stepwise thermal demagnetizations reveal two stable components. One of them is aligned to the present-day field direction and presents maximum unblocking temperatures ranging between 200 and 250°C. A well-defined second component called component A unblocks at 450-475°C and can be destroyed at low peak fields via AF demagnetization (fig. 2). Component A shows high clustering at site level (Table 1). The demagnetization features and the rock magnetic experiments suggest that this component is carried by magnetite. The component A has been considered the characteristic remanent magnetization (ChRM) and presents a systematic normal polarity (fig. 2, Table 1). As demonstrated by Torres-López et al. (2014) in Sinemurian to Bathonian limestones (same as this work) and Moussaid et al. (2014) in Bathonian to Albo-Cenomanian red beds, the ChRM component in the Central High Atlas corresponds to a widespread Cretaceous remagnetization occurred at the age between 80 to 110 Ma, most likely 100 Ma. The age has been calculated comparing the remagnetization direction obtained by the small circle intersection (SCI) method (Waldhör &

Appel, 2006) with the global apparent polar wander path (GAPWP) in Africa coordinates. (Torres-López *et al.*, 2014; Moussaid *et al.*, 2014), also considering the normal polarity of remagnetization within the Cretaceous superchron. The hysteresis parameters of the analysed limestones are in the Superparamagnetic-Single domain mixing zone of the Day plot (Torres-López *et al.*, 2014), typical of chemically remagnetized limestones (Dunlop, 2002).

Interpretation: Reconstruction of fold geometry at 100 Ma

Remagnetization occurred at the Early-Late Cretaceous boundary, during the period of tectonic quiescence between the two main stages of tectonic evolution of the Central High Atlas (i.e. basinal stage during the Triassic-Jurassic and inversion during the Late Cretaceous-Cenozoic). This allows filtering the compressional Late Cretaceous-Cenozoic folding and separate these structures from the ones predating the remagnetization stage. In order to define the attitude of bedding at the remagnetization stage, we must restore it to its position during the time of remagnetization (paleodips) applying the method developed by Villalaín et al. (2003, 2015). This consists in rotating the magnetic directions of each site around the strike of bedding until the paleomagnetic mean vector reaches the expected (or reference) direction. The dip of beds after this rotation represents the paleodip at the moment of remagnetization. The characteristic direction of remagnetization (or reference direction) was obtained by SCI method (Waldhör and Appel, 2006) and subsequently compared with the expected paleomagnetic direction obtained from the GAPWP in NW African coordinates (Torsvik et al., 2012) that shows declination and inclination values of D = 336°, I =38° for the Imilchil region. Once the paleodips at the time of remagnetization were obtained (Table 1), they were projected onto the vertical plane of the cross sections considering the stratigraphic position of samples within the sedimentary pile. Cross-sections including these dips will show a picture of each structure at the remagnetization time (100 Ma). Conversely to other geological conventional methods (i.e. growth strata analysis), this is a unique technique that permits quantifying the dip of beds at this particular moment in the history of the region (Table 1).

A common feature for the three studied cases (figs. 3, 4, 5) is that the pre-Cenozoic geometry of the anticlines is different from the present-day cross-section and does not fit with a pre-tectonic horizontal geometry, either. Considering the three cases separately, reconstruction of the Tasraft anticline to its Cretaceous geometry (fig. 3) indicates that both limbs of the anticline were already almost symmetrical and showed moderate to steep dips, without smaller scale folds and a slight southward vergence which developed later in the evolution of the structure, together with the increase in dip of both limbs.

The Tassent anticline shows an asymmetric geometry in its present-day profile (fig. 4) with a larger and generally steeper southern limb and, consequently, a slight southward vergence. The restored cross-section shows a more symmetric and narrower shape, specially in its lower part.

The geometry of the Tissila anticline is asymmetric (fig. 5), and in this case, the vergence is towards the north. Its northern flank shows a thicker preserved sequence of Jurassic units than its southern flank does, which suggests the presence of a basement fault with an uplifted southern wall. The main changes between the present-day and the restored cross-section lie in the development and geometry of the syncline located to the North of the Tissila anticline, which shows longer limbs in the present-day cross-section.

Paleomagnetic data thus indicate that the three studied structures were already partially formed at 100 Ma and underwent different evolutionary trends: Tasraft, having dips of up to 49° on the southern flank, in the pre-Late Cretaceous stage; Tassent, whose dips at the remagnetization stage, reaching 80-90°, were slightly higher than in the present-day cross-section, and Tissila with dips of up to 70º at the moment of the remagnetization and a strong asymmetry both in the pre- and the post-remagnetization stages.

The relation between the restored and in situ dips allows for observing the contribution of folding in the three structures before and after 100 Ma (i.e. pre and post-remagnetization folding) (fig. 6.A), that implies a certain degree of building of the chain before the Cenozoic compressional stage.

Discussion: timing and origin of folding in the Central High Atlas.

To ensure a correct restoration, the assumption of coaxiallity of structures formed during the pre- and post-remagnetization stages must be checked. This can be performed by plotting bed orientations of limbs whose dips majoritarily formed during the pre-remagnetization stage (i.e. unfolding angle ϕ <30% of the present day bedding), on one side and limbs whose tilting developed essentially during the compressional (i.e. ϕ >70% of the present day bedding), post-remagnetization folding stage, on the other (Fig. 6.B). The resulting plot indicates an almost perfect coaxiallity between both types of structures, that is coherent with the tectonic evolution of the Central High Atlas resulting from basement faulting and extensional rifting followed by compressional folding/faulting (Laville *et al.*, 2004; El Harfi *et al.*, 2006).

The timing of folding inferred from paleomagnetic data strongly contrasts with models for the Central High Atlas assuming an almost flat geometry before the Cenozoic compression (Beauchamp *et al.*, 1999; Teixell *et al.*, 2003; Arboleya *et al.*, 2004). According to our reconstructions, most part of the Central High Atlas showed intermediate dips already at 100

Ma, and possibly this early structuring also conditioned the subsequent evolution of structures.

Although remagnetizations give reliable information about the stages of folding and provide a way to clearly separate two tectonic stages, the mechanisms responsible for the pre-Cretaceous geometry are not easy to unravel, because a combination of uplift by magma intrusion, diapirism, and shortening is expected to be found in different proportions. Despite having dips of up to 50° the shape of the Tasraft anticline (fig. 3) prior to the Cenozoic is likely more consistent with the salt and shale migration of the Triassic ductile detachment. In the Tassent anticline, changes in the position of the syncline hinges at both sides of the anticline are necessary to explain its evolution from the Cretaceous to the present-day geometry. The narrower shape and steeper dips in the case of the Tassent anticline prior to the Cenozoic compression (fig. 4) are consistent with an origin related to magmatic intrusions linked to underlying basement faults, but ductile flow in its core is also necessary for hinge migration during the Cenozoic and necking responsible for dip decrease at its limbs (see Charrière *et al.*, 2009; Michard *et al.*, 2011). For the Tissila anticline, only the hinge of the northern syncline migrated between the two stages; in our interpretation, the southern one was likely fixed because of the strong control imposed by the basement fault underlying the southern limb of the anticline having a thinner *décollement*.

The results obtained have important implications in the interpretation of the tectonic style of the Central High Atlas. In a percentage of structures, the present-day tilting of beds is not only a consequence of Cenozoic shortening (that should be therefore recalculated) but the effect of its combination with previous folding due to salt flow and/or magma intrusions (or a combination of both, since temperature increase can influence the viscosity of salt, see e.g. Schofield, 2014 and references therein).

Conclusions

The analysis of directions of a Cretaceous remagnetization observed in the Central High Atlas allows the folding that occurred before 100 Ma to be quantified. The results obtained indicate different evolutions for the studied folds; the present-day limbs of the Tassent anticline were already tilted at the beginning of the Late Cretaceous, whereas in the Tasraft anticline, about 50% of the present-day dip was acquired after the remagnetization stage (fig. 6). The Tissila anticline shows an intermediate position, with a partially developed limb that grew northwards by migration of the hinge of the adjacent syncline. This finding means that folding during the Mesozoic, basinal stage was heterogeneously distributed along the chain and that each individual fold must be considered separately. The technique applied for fold reconstruction shows promising results that, in further works, may result in a paleostructure map of the High Atlas at 100 Ma The relationship between the studied structures and their diapiric/magmatic cores and particular features of their evolution indicates that diapiric processes and intrusions present at the Central High Atlas are involved in the formation of the anticlines, with probable contribution of both of these processes in the different structures.

Acknowledgements

The authors are grateful to Ruth Soto, Dominique Frizon de Lamotte, Bernard Housen, Antonio Teixell and David Westerman for their fruitful comments. Funding for this work came from project CGL2012-38481 of the Ministerio de Economía y Competitividad of the Spanish government and European Regional Development Fund. Sara Torres-López acknowledges the financial support given by the FPI grant of the Ministerio de Economía y Competitividad (Spanish government).

References

Arboleya, M.L., Teixell, A., Charroud, M. and Julivert, M., 2004. A structural transect through the High and Middle Atlas of Morocco: tectonic implications. *Journal of African Earth Science*. **39**, 319– 327.

Armando, G., 1999. Intracontinental alkaline magmatism: Geology, Petrography, Mineralogy and Geochemistry of the Jbel Hayim Massif (Central High Atlas-Morocco). Mémoires de Géologie de l'Université de Lausanne 31, 106.

Beauchamp, W., Allmendinger, R., Barazangi, M., Demnati, A., El Alji, M. and Dahmani, M., 1999. Inversion tectonics and the evolution of the High Atlas Mountains, Morocco, based on a geological-geophysical transect, *Tectonics*, **18**, 163–184, doi: 10.1029/1998TC900015.

Bensalah, M.K., Youbi, N., et al., 2013. The Jurassic–Cretaceous basaltic magmatism of the Oued El-Abid syncline (High Atlas, Morocco): Physical volcanology, geochemistry and geodynamic implications. *Journal of African Earth Sciences*, **81**, 60–81.

Charrière, A., Haddoumi, H., Mojon, P.-O., Ferrière, J., Cuche, D. and Zili, L., 2009. *Mise en évidence par ostracodes et charophytes de l´âge paléocène des dépôts discordants sur les rides anticlinales de la région d'Imilchil (Haut Atlas, Maroc); conséquences paléogéographiques et structurales*. Comptes Rendus. Palevol., **8**, 9–19.

Dunlop, D.J. 2002. Theory and application of the Day plot (Mrs/Ms versus Hcr/Hc): 2. Application to data for rocks, sediments, and soils. *Journal of Geophysical Research*, **107**, http://dx.doi.org/10.1029/2001JB000487.

El Harfi, A., Guiraud, M. and Lang, J., 2006. Deep-rooted "thick skinned" model for the High Atlas Mountains (Morocco). Implications for the structural inheritance of the southern tethys passive margin. *Journal of Structural geology*. 1958-1976.

Fadile, A., 1987. Carte géologique du Maroc au 1/100.000 : feuille d'Imilchil. Notice explicative. Notes et Mémoires du Service Géologique du Maroc, nº 397.

Fisher, R.A., 1953. Dispersion on a sphere. Proceedings of the Royal Society of London, Series A, 217, 295–305.

Frizon de Lamotte, D., Saint Bézar, B., Bracène, R. and Mercier, E. 2000. The two main steps of the Atlas building and geodynamics of the western Mediterranean. *Tectonics*, **19**, 740–761.

Frizon de Lamotte, D., Zizi, M., Missenard, Y., Hafid, M., El Azzouzi, M., Maury, R.C., Charrière, A., Taki, Z., Benammi, M. and Michard, A. 2008. Chapter 4: *the Atlas System. In: Continental Evolution: The Geology of Morocco* (A. Michard, O. Saddiqi, A. Chalouan and D. Frizon de Lamotte, eds). Lect. Notes Earth Sci., 116, 133.

Frizon de Lamotte, D., Raulin, C., Mouchot, N., Wrobel-Daveau, J.C., Blanpied and C., Ringenbach, J.C. 2011. The southernmost margin of the Tethys realm during the Mesozoic and Cenozoic: initial geometry and timing of the inversion processes. *Tectonics*, **30**, TC3002.

Guezal, J., El Baghdadi, M., Barakat, A. and Raïs, J. 2011. Le magmatisme jurassique-crétacé de Béni-Mellal (Haut- Atlas central, Maroc) : géochimie et signification géodynamique. *Bulletin de l'Institut Scientifique, Sciences de la Terre*. **33**, 17-23.

Laville, E., 1985. Evolution sédimentaire, tectonique et magmatique du bassin Jurassique du Haut Atlas (Maroc): modèle en relais multiples de décrochements. Thèse Doct. Etat, Univ. Sci. Tech. Languedoc, Montpellier, 166 p.

Laville, E. and Piqué, A. 1992. Jurassic penetrative deformation and Cenozoïc uplift in the Central High Atlas (Morocco): a tectonic model. Structural and orogenic inversions. *Geologishe Rundschau*. **81**, 157–170.

Laville, E., Zayane, R., Honnorez, J. and Piqué, A. 1994. Le métamorphisme jurassique du Haut Atlas central (Maroc); épisodes synschisteux et hydrothermaux. *Comptes Rendus de l'Académie des Sciences de Paris*. **318**, 1349–1356.

Laville, E., Piqué, A., Amrhar, M. and Charroud, M. 2004. A restatement of the Mesozoic Atlasic Rifting (Morocco). *Journal of African Earth Sciences*, **38**. 145-153.

Lhachmi, A., Lorand, J.P. and Fabries, J. 2001. Pétrologie de l'intrusion alcaline mésozoïque de la région d'Anemzi, Haut Atlas Central, Maroc. *Journal of African Earth Sciences*. **32** (4), 741–764.

Michard, A., Frizon de Lamotte, D., Saddiqi, O. and Chalouan, A. 2008. An outline of the geology of Morocco, in Continental Evolution: The Geology of Morocco, In: *Lecture Notes in Earth Science*. (A. Michard, O. Saddiqi, and A. Chalouan, eds), **116**, 1–31, doi:10.1007/978-3-540-77076-3_1, Springer, Berlin.

Michard, A., Ibouh, H. and Charrière, A., 2011. Syncline-topped anticlinal ridges from the High Atlas: A Moroccan conundrum, and inspiring structures from the Syrian Arc, Israel. *Terra Nova*. **23**, 314–323.

Moussaid B., Villalaín J.J., Casas-Sainz A., El Ouardi H., Oliva-Urcia B., Soto R., Román-Berdiel T. and Torres-López S. 2015. Primary vs. secondary curved fold axes: Deciphering the origin of the Aït Attab syncline (Moroccan High Atlas) using paleomagnetic data. *Journal of Structural Geology*. **70**, 65-77.

Piqué, A., Charroud, M., Laville, E., Aït Brahim, L. and Amrhar, M. 2000. The Tethys southern margin in Morocco; Mesozoic and Cainozoic evolution of the Atlas domain. *Mémoires du Muséum national d'histoire naturelle*. **182**, 93-106.

Saura, E., Vergés, J., Martín-Martín, J.D., Messager, G., Moragas, M., Razin, P., Grélaud, C., Joussiaume, R., Malaval, M., Homke, S. and Hunt, D.W. 2014. Syn- to post-rift diapirism and minibasins of the Central High Atlas (Morocco): the changing face of a mountain belt. *Journal of the Geological Society, London*. **171**, 97– 105.

Schofield, N., Alsop, I., Warren, J., Underhill, J.R., Lehné, R., Beer, W. and Lukas, V. 2014. Mobilizing salt: Magma-salt interactions. *Geology*, **42**, 599-602.

Soto, R., Casas-Sainz, A.M., Villalaín, J.J., Gil-Imaz, A., Fernández-González, G., del Río, P, Calvo, M., and Mochales, T. 2008. Characterizing the Mesozoic extension direction in the Northern Iberian Plate margin by anisotropy of magnetic susceptibility (AMS). *Journal of the Geological Society of London* .**165** (6), 1007-1018.

Soto, R., Casas-Sainz, A.M. and Villalaín, J.J. 2011. Widespread Cretaceous inversion event in northern Spain; evidence from subsurface and Paleomagnetic data. *Journal of the Geological Society, London*. **168**, 899-912.

Teixell, A., Arboleya, M.L., Julivert, M. and Charroud, M. 2003. Tectonic shortening and topography in the Central High Atlas (Morocco). *Tectonics*, **22**, 1051.

Tesón, E., Pueyo, E. L., Teixell, A., Barnolas, A., Agustí, J. and Furió, M. 2010. Magnetostratigraphy of the Ouarzazate Basin: Implications for the timing of deformation and mountain building in the High Atlas Mountains of Morocco. *Geodinamica Acta*, **23** (4), 151-165.

Torres-López S., Villalaín, J.J., Casas, A., El Ouardi, H., Moussaid B. and Ruiz-Martínez V.C. 2014. Widespread Cretaceous secondary magnetization in the High Atlas (Morocco). A common origin for the Cretaceous remagnetizations in the western Tethys?.*Journal of the Geological Society*. **171**, 673-687.

Torsvik, T. H., Van der Voo, R., Preden, U., Mc Niocaill, C., Steinberger, B., Doubrovine, P. V., Van Hinsbergen, D., Domeier, M., Gaina, C., Tohver, E., Meert, J. G., McCausland, P.J.A. and Cocks, L.R.M. 2012. Phanerozoic polar wander, palaeogeography and dynamics. *Earth-Science Reviews*, **114**, 325-368.

Villalaín, J.J., Fernández-Gonzalez, G., Casas, A.M., and Gil-Imaz, A. 2003. Evidence of a Cretaceous remagnetization in the Cameros Basin (North Spain): implications for basin geometry. *Tectonophysics*, **377**, 101–117.

Villalaín, J.J., Casas-Sainz, A.M. and Soto, R. 2015. Reconstruction of inverted sedimentary basins from syn-tectonic remagnetizations. *Geological Society, London, Special Publication*, **425.** doi.org/10.1144/SP425.10

Waldhör, M. and Appel, E. 2006. Intersections of remanence small circles: new tools to improve data processing and interpretation in palaeomagnetism. *Geophysical Journal International*. **166**, 33–45.

Zayane, R., Essaifi, A., Maury, R.C., Piqué, A., Laville, E. and Bouabdelli, M. 2002. Cristallisation fractionnée et contamination crustale dans la série magmatique jurassique transitionnelle du Haut Atlas central (Maroc). *Comptes Rendus Geoscience, Paris*. **334**, 97–104.

Figure Captions

Figure 1. A) DEM and geological sketch with the situation of the Central High Atlas and Imilchil area. B) Geological map of the Imilchil region, the sampling sites and the situation of the three restored profiles corresponding to figures 3, 4 and 5. Modified from Torres-López et al., (2014).

Figure 2. NRM thermal and alternating field demagnetizations of representative samples. All directions are plotted with their in-situ coordinates. Open symbols are projections of the vector end points onto the vertical north–south plane, and filled symbols are projections onto the horizontal plane. The evolution of normalized NRM intensity M/M_0 is shown in the insets.

Figure 3. A) Present-day geological profile of the Tasraft anticline. The paleomagnetic sites, bedding (black lines) and paleomagnetic vectors (arrows) are indicated. B) Restored section of the Tasraft anticline to 100 Ma. C) Geological sketch showing the location of the studied transect and the paleomagnetic sites (based on Fadile, 1987). D) Stereoplot showing the small circles corresponding to the restored remagnetization directions from selected sites. Squares are directions of the in situ remagnetization for each site. Triangles represent the optimum directions of remagnetization for each site. Circles show the paleomagnetic

direction of remagnetization after complete bedding correction. The 95% confidence circles are also represented. Paleomagnetic vectors have been projected onto the vertical plane of the cross-section, and the inclinations shown in this figure are therefore apparent inclinations. The green line in the restored section represents the restored topography.

Figure 4. A) Present-day Tassent geological profile. B) Restored section to 100 Ma. C) Geological sketch showing the transect studied and the paleomagnetic sites (based on Fadile 1987). D) Stereoplot showing small circles corresponding to the restored remagnetization directions from selected sites. Symbols are the same as those shown in fig. 3.

Figure 5. A) Present-day cross-section of the Tissila anticline. The paleomagnetic sites, bedding and paleomagnetic vectors are indicated. B) Restored section to 100 Ma. C) Geological sketch showing the transect studied and the paleomagnetic sites (based on map of Imilchil, Fadile 1987). D) Stereoplot showing the small circles corresponding to the restored remagnetization directions from selected sites. Symbols are the same as those shown in fig. 3.

Figure. 6. a) Plot showing the relationship between present-day dips and Cretaceous (~100 Ma) dips at the limbs of the three structures studied in the High Atlas. Points plotted along the abscise axis correspond to those sites whose tilt was totally acquired after the Late

Cretaceous (i.e., beds were horizontal before the Cenozoic), and points plotted on the diagonal correspond to sites whose present tilt was acquired before the remagnetization (Late Cretaceous) stage. The distance to the abscise axis is related to the part of the structure that was already formed at the Late Cretaceous. Negative values for the ordinate axis indicate dips during the Late Cretaceous with the dip sense opposite to the present-day, in situ sense of dip. Small equal area diagram showing the optimum direction of the remagnetization, after bedding correction and in situ are also shown for the three cases differentiated in the figure. b) Stereoplots showing the poles to bedding in the Imilchil area (Torres-López et al., 2014) for dips acquired mostly during the pre-inversion stage (i.e. the unfolding for restoration to the paleofield direction is <30% of the present day bedding, left) and for compressional, Cenozoic tilting (i.e. unfolding is >70% of the present day bedding, right). Folds axes obtained are also shown.

Table 1. Remanent Magnetization parameters for the Characteristic Component. The present day and the restored bedding to the 100 Ma paleofield direction (restored bedding) are also indicated. DD/D, dip direction and dip; N/n, number of sample directions used in the analysis vs. number of samples demagnetized; K and α_{95}, Fisher statistical parameters (Fisher, 1953); D and I, declination and inclination; ϕ, unfolding angle for restoration to the paleofield direction.

Profile	Azimut	Site	Age	Lat º	Lon º	In Situ Bedding	N/n	In Situ				100% Tilt Corrected				Corrected to			Restored bedding	
						DD/D										D 336º I 38º			DD/D	
						Dip dir, Dip		D	I	K	α95	D	I	K	α95	D	I	**Φ**	Dip dir	Dip
		IG1	Aalenian	32.207	5.825	123, 40	10/10	329.4	-7.0	373.5	3.5	335.6	34.5	356.7	3.5	337.3	39.2	44.1	303	4
		IG2	Aalenian	32.208	5.828	130, 57	7/8	334.4	22.4	108.9	7.3	20.0	66.0	94.0	7.3	338.6	38.3	16.4	130	41
		IG3	Aalenian	32.208	5.828	314, 24	6/8	55	63.1	81.5	7.5	11.4	58.2	81.4	7.5	345.6	34.6	59.3	134	35
		IG4	Aalenian	32.208	5.828	320, 13	6/8	342.8	38.4	52.7	10.6	339.8	26.3	52.7	10.6	342.0	38.0	2.7	320	10
Tasraft	320	IG5	Aalenian	32.208	5.828	340, 10	5/8	15.6	70	54.7	12.5	4.5	61.3	151.9	7.5	354.3	41.5	36.5	160	27
		IG6	Bajocian	32.205	5.822	129, 60	10/10	330	-0.1	139.7	8.2	346.4	53.9	90.6	8.2	336.3	39.8	42.1	129	18
		IG10	Bajocian	32.165	5.943	304,46	10/10	18.3	64.7	98.6	6.1	333.4	33.0	98.6	6.1	336.0	40.1	39.1	304	7
		IG14	Bajocian	32.170	5.949	120,7	7/8	354.8	32.9	27.1	13.1	358.9	36.7	27.2	13.1	347.5	23.9	18.1	120	25
		IG15	Bajocian	32.166	5.945	331,26	8/8	342.4	58.4	76.1	6.4	338.1	32.7	76.1	6.4	338.6	39.6	20.6	331	5
		IG20	Aalenian	32.208	5.829	125,60	8/9	328.2	32.1	114.9	2.8	46.7	70.2	113.2	2.8	331.4	41.8	10.8	125	49
		IC-4	Bathonian	32.162	5.630	348, 22	8/8	331.4	45.1	44.7	13.9	335.3	23.8	44.5	13.9	333.3	37.4	8.0	348	14
		IC-5	Bajocian	32.208	5.640	168, 54	7/9	341.2	2.8	66.2	6.4	335.7	56.2	57.8	6.4	339.3	38.9	36.5	168	15
		IC-6	Bajocian	32.207	5.695	155, 35	8/10	338.2	22.7	102.8	5.5	340.5	57.6	132.1	5.5	338.8	38.3	15.5	155	19
		IC-7	Aalenian	32.214	5.697	149, 81	8/10	338.6	49.2	74.9	6.4	139.4	49.0	74.8	6.4	337.0	38.3	9	149	90
Tassent	353	IC-13	Toarcian	32.225	5.704	343, 33	7/8	336.2	31.7	1132.1	1.8	337.2	-1.1	1202.0	1.8	335.6	38.2	6.5	343	26
		IC-14	Aalenian	32.269	5.643	355, 40	8/10	317.2	55.6	187.8	4.4	333.3	20.2	186.4	4.4	330.1	34.8	24.1	355	16
		IC-15	Aalenian	32.299	5.657	164,09	8/8	339.4	28.8	1665.2	1.6	338.9	37.8	1681.8	1.6	338.8	38.7	9	164	0
		IC-16	Aalenian	32.330	5.665	004,00	8/8	331.4	42.6	312.9	4.3	331.4	42.6	312.9	4.3	334.3	36.7	7	184	7
		IC-70	Aalenian	32.220	5.701	348,61	6/9	339	22	48.2	9.8	337.4	-38.3	48.1	9.8	337.3	38.5	17	348	78
		IC-44	Bathonian	32,150	5,579	115, 57	7/8	322.5	20.3	11.7	12.5	4.5	62.5	11.7	12.5	331.5	43.3	26.9	115	30
		IC-45	Bathonian	32,141	5,569	090, 25	7/8	356.8	51.4	63.95	7.6	25.6	46.3	63.5	7.6	333.6	45.9	20.8	90	4
		IC-46	Bathonian	32.135	5.560	324, 49	5/8	56.1	76.3	122.9	6.9	342.0	40.1	128.7	6.9	341.2	36.8	52.4	144	3
Tissila	332	IC-47	Bathonian	32.118	5.550	342, 85	7/8	330.4	52.2	52.0	9.4	333.6	-32.0	52.0	9.4	333.0	37.8	14.6	342	70
		IC-48	Toarcian	32.105	5.530	161, 51	7/8	330.5	3.4	85.8	7.3	323.3	53.1	54.1	7.3	327.9	36.6	33.9	161	17
		IC-64	Toarc-Aalenian	32.102	5.514	115,19	7/8	328.5	35.5	284.9	3.6	339.8	50.4	286.4	3.6	332.5	42.5	8.5	115	10
		IC-65	Toarc-Aalenian	32.110	5.550	340,60	8/8	331.4	63.4	134.7	4.8	336.2	3.7	135.0	4.8	335.1	38.2	25.3	340	35